



Study on High-Temperature Mechanical Properties and Forming Limit Diagram of 7075 Aluminum Alloy Sheet in Hot Stamping

Ruiying Gu, Qi Liu, Shichao Chen, Wurong Wang, and Xicheng Wei

(Submitted January 4, 2019; in revised form September 10, 2019; published online November 25, 2019)

To improve the formability of aluminum alloy sheets and avoid springback, a newly developed forming technique, HFQ (heat-forming-quenching), has attracted attention in the automobile industry. In this work, a high-temperature tensile test and the Nakazima hemispherical punch method were used to simulate the HFQ process to study the high-temperature flow behavior and formability of 7075-T4 aluminum alloy sheet. The results demonstrated that elongation to fracture was positively correlated with temperature, changing from 15% in the quenching state to 26.1% at 440 °C. Strain rate sensitivity was found to vary according to the strain rate due to the coupled competition between temperature and the strain rate. It was concluded that the necking to shear fracture transition of 7075 based on HFQ occurred at 358 °C. In addition, the forming limit of the alloy sheet decreased with the increasing waiting time. The temperature field distribution of the alloy sheet for different waiting times at a forming velocity of 10 mm/s was obtained by thermomechanical coupled simulations. Different modes of rupture indicated different thermomechanical behaviors due to the different initial temperatures under hot stamping.

Keywords 7075-T4 aluminum alloy sheet, FLD, Flow behavior, HFQ, NTSF transition

1. Introduction

Due to the stringent greenhouse gas emission standards and comprehensive promotion of the substitution of renewable-energy vehicles for traditional-fuel vehicles, an increasing number of automotive industries have emphasized their strategies of using lightweight materials to achieve fuel efficiency, emissions reduction and product recyclability (Ref 1). Within the last decade, 7000 series (Al-Zn-Mg-Cu) aluminum alloys have attracted many researchers' attention as a mass-saving replacement for some high-strength steels due to their excellent strength-to-density ratio, bend stiffness and corrosion resistance. Nevertheless, poor formability at room temperature (RT), high springback and high cost are the problems encountered in the application of 7000 series aluminum alloys. Therefore, various advanced hot forming processes are now under investigation to solve these problems. Heat-forming-quenching proposed by Garrett et al. (Ref 2) is one such promising hot processing technology that ensures the accurate fabrication of complex automotive parts and is applicable to any aluminum alloy sheet. This approach consists of a solution heat treatment

(SHT) and subsequent hot stamping, followed by cold mold quenching. Compared with the traditional hot stamping process, holding the formed part in a water-cooling mold after hot forming has the advantage of eliminating thermal distortion and springback.

In recent years, considerable efforts have been made in the HFQ process field, primarily on 5754-O, 6082 and 7075-T6 (Ref 3–5) alloy sheets. The world's first HFQ-based aluminum hot forming line for the automotive industry was developed by AP&T Sweden AB in 2016. Ying et al. (Ref 6) studied the rheological curves of the 7075-T6 aluminum alloy at high temperature based on the HFQ process using the GTN mesoscopic damage model. The results showed that the initial pore volume fraction, pore volume fraction of nucleation particles and aggregate pore volume fraction had significant effects on the fracture behavior and that the fracture pore volume fraction had little effect on the fracture point. Zheng et al. (Ref 7) explored the effects of different heat treatment conditions on the mechanical properties and microstructure of the 7075-T6 aluminum alloy sheet. The best heat treatment window of 7075-T6 was at 475 °C for 30 min, and the alloy was rapidly quenched at a rate of 50 °C/s, followed by an artificial aging treatment at 120 °C for 24 h to obtain the best mechanical properties of the material. Ying et al. (Ref 8) studied the interfacial heat transfer coefficient (IHTC) of 7075-T6 and H13 steels under hot stamping conditions. IHTC was affected by the contact pressure, roughness and lubricant condition. IHTC decreased with an increase in roughness and increased with increasing contact pressure.

Despite the numerous research results for various aluminum alloys obtained in studies carried out to date, most academics neglect the pronounced microstructure evolution deviation caused by inexact experimental schemes. Some researchers have even conducted tensile tests using the traditional high-temperature experiment method, and the results were completely different from the results of the HFQ process. On the

Ruiying Gu, Qi Liu, and Shichao Chen, School of Materials Science and Engineering, Shanghai University, Shanghai, People's Republic of China; and Wurong Wang and Xicheng Wei, School of Materials Science and Engineering, Shanghai University, Shanghai, People's Republic of China; and State Key Laboratory of Advanced Special Steel, Shanghai University, Shanghai, People's Republic of China. Contact e-mail: wrwang@shu.edu.cn.

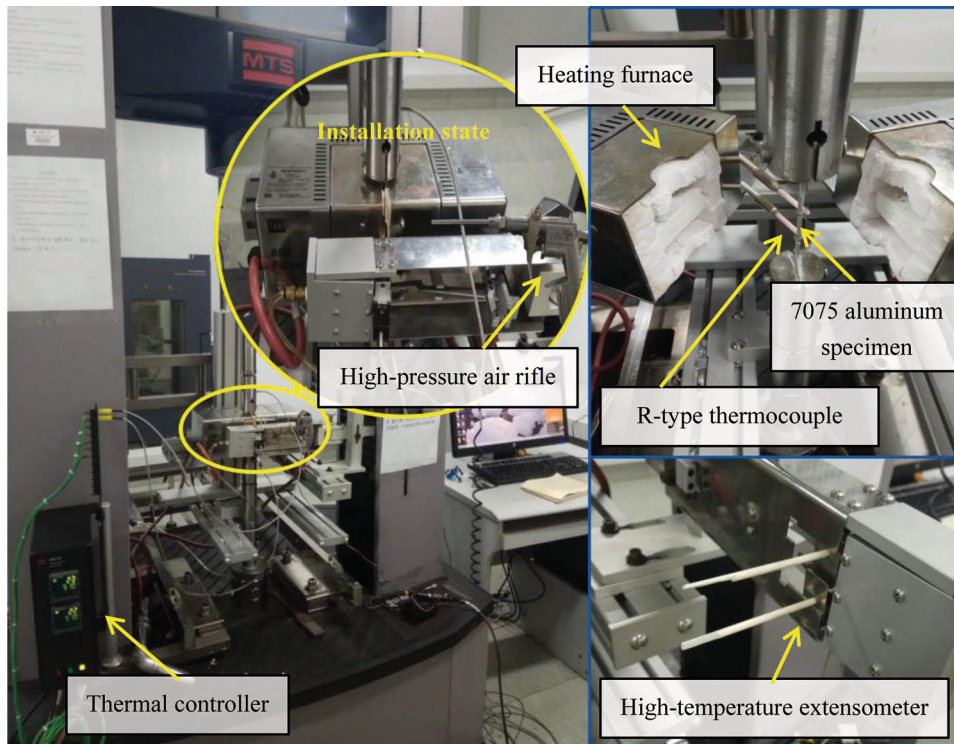


Fig. 1 Experimental setup of the high-temperature tensile test

Table 1 Chemical composition of the 7075-T4 aluminum alloy sheet

Element	Zn	Mg	Cu	Cr	Fe	Al
wt.%	6.10	2.54	1.20	0.20	0.20	Bal.

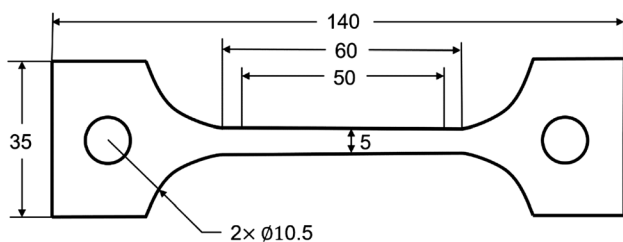


Fig. 2 Schematic diagram of the high-temperature tensile specimen (unit: mm)

one hand, some researchers only soaked specimens for 5 min in the high-temperature tensile test. Previous research by Liu et al. (Ref 9) found that a solution heat treatment of 440 °C applied for 30 min ensured that the coarse phases maximally redissolved back to the aluminum matrix to ensure that the strength of the part could be significantly improved after aging, reaching as high as 538 MPa. On the other hand, the faster the cooling rate, the greater the age-strengthening effect because a high cooling rate prevents the precipitation of coarse secondary phases, thus reducing the loss of supersaturation. To solve this

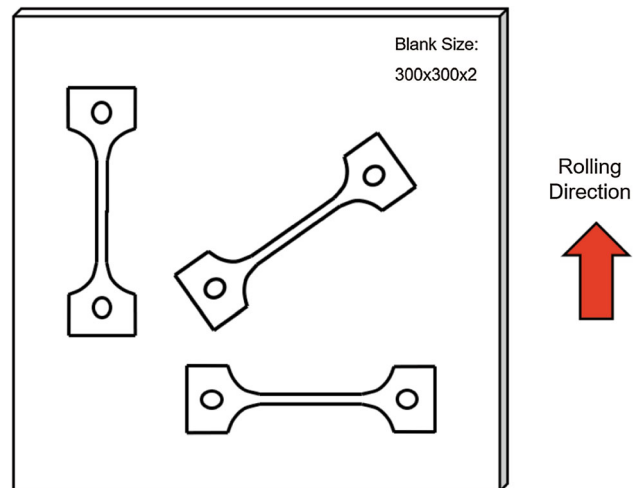


Fig. 3 Cutting program of the specimen (unit: mm)

gap in the current literature, experimental schemes must be redesigned to guarantee that the experimental procedure can be as close as possible to the actual manufacturing process. In this study, a solution heat treatment of 510 °C for 30 min, quenching by a high-pressure air rifle and artificial aging at 120 °C for 24 h were chosen as the optimal heat treatment combination for the 7075 aluminum alloy during sheet metal stamping.

Yan et al. (Ref 10) studied the rheological behavior of Al-Zn-Mg-Cu alloys under high-temperature uniaxial tensile tests. It was found that the flow stress curve decreased with increasing deformation temperature and decreased with a decrease in the strain rate. Gourdet et al. (Ref 11) found that

the 7075 aluminum alloy mainly underwent continuous dynamic recrystallization during thermal deformation. The grain size is significantly reduced with continuous dynamic recrystallization, resulting in a very fine grain structure, which significantly improves the mechanical properties of the aluminum alloy material. To apply the high-temperature flow curves to the finite element numerical simulation, it is crucial to establish a constitutive equation that can accurately describe the high-temperature rheological properties of the aluminum alloy sheet in the strengthened state. Zhuang et al. (Ref 12) established a constitutive equation for the viscoplastic continuum damage to the 7075-T6 aluminum alloy over the temperature range of 350 to 420 °C based on the microscopic and macroscopic mechanical properties. Senthil et al. (Ref 13) established the constitutive equation for the 7075 aluminum alloy rod based on the Johnson–Cook model and the failure model that was verified by ballistic impact testing.

The formability of 7075 aluminum alloy sheets has been extensively discussed in the literature. Huo et al. (Ref 14) investigated the formability of a 7075 alloy sheet under the conventional hot stamping process using the Erichsen test and found that the maximal drawing depth was 10.8 mm at 200 °C. Barnwal et al. (Ref 15) studied the relationship among the anisotropy, strain path and formability of the AA6061 aluminum alloy sheet using hemispherical punch bulging experiments and found that formability was related to the specific texture volume. In this study, the contact sequence between the

blank and the tools is taken into consideration. The major and the tiny features on the same accessory may experience entirely different forming environments. Therefore, different initial forming temperatures of the different regions in the forming sequence were taken into consideration. In addition, few studies on the fracture mode transition under the HFQ process are available. The quenching temperature at which a necking fracture transforms into a shear fracture, which is defined as evidence of the fracture behavior in the hemispherical punch test, was investigated by SEM observations.

The high-temperature forming limit diagram (FLD) of the aluminum alloy sheet is very important for evaluating the formability of the aluminum alloy in the hot stamping process. The concept of the FLD proposed by Keeler et al. (Ref 16) and supplemented by Goodwin (Ref 17) can reflect the ultimate deformation ability of a metal sheet. The FLD is constructed by changing the shape of the sample to obtain different loading states and different strain paths. Huang et al. (Ref 18) obtained the 7075-T6 aluminum alloy sheet FLD under isothermal

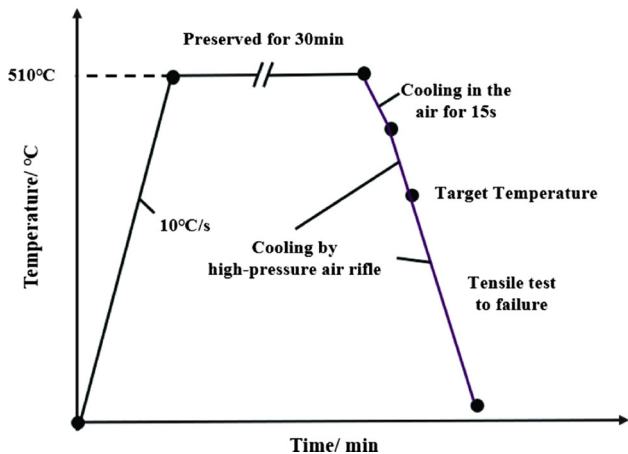


Fig. 4 Experimental program for the high-temperature tensile test based on the HFQ process

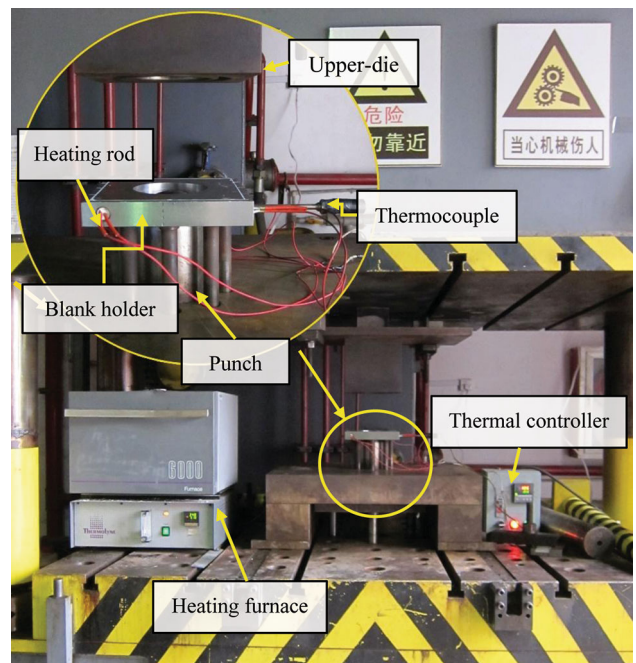


Fig. 6 Experimental setup of the high-temperature hemispherical punch test

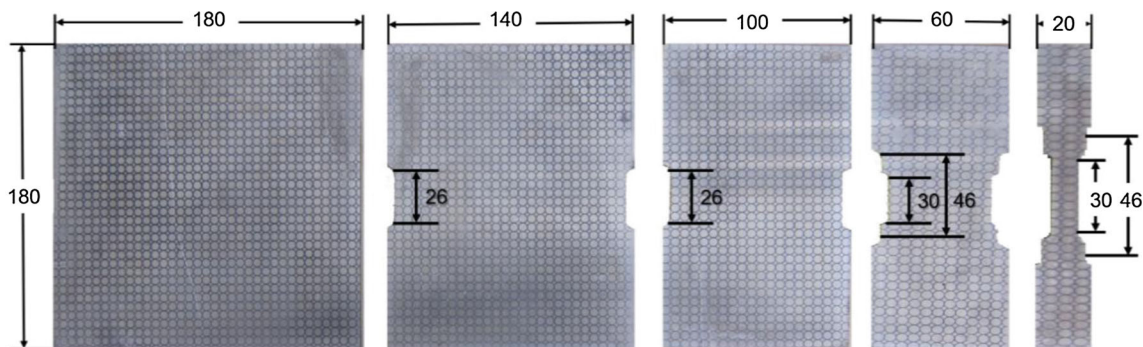


Fig. 5 Samples of 7075 with different widths for the FLD tests (unit: mm)

conditions between 50 and 280 °C. They found that the FLD of the 7075-T6 aluminum alloy sheet was significantly affected by the temperature and the forming limit increased with increasing temperature. The FLD increased dramatically at temperatures between 150 and 200 °C. Additionally, the fracture type of the specimens changed from a wide range of brittle fracture to a ductile necking fracture as the temperature increased. Mohamed et al. (Ref 19) studied the effect of the swell of hemispherical rigid embossing on the rupture type of an AA6082 aluminum alloy sheet at a deformation temperature of 470 °C at stamping velocities that varied from 0.166 to 0.64 m/s. It was found that the specimens tended to circumferentially rupture at a low stamping velocity, while the part tended to radially rupture at a high stamping velocity.

In this study, a high-temperature tensile test of 7075 aluminum alloy sheets based on the HFQ process was performed to determine the effects of temperature, strain rate and anisotropy on the tensile behavior. High-temperature hemispherical punch tests at different velocities and waiting times were carried out to optimize the forming process parameters. The fracture mechanism and microstructure evolution were analyzed by the OM and SEM methods.

2. Materials and Methods

2.1 High-Temperature Tensile Test

A high-temperature uniaxial tensile test was conducted on the MTS C45.305E electronic material testing system, as shown in Fig. 1. The specific devices used in the tests were a tensile testing machine, a furnace and a temperature controller. Temperature monitoring was carried out using two R-type thermocouples that were placed symmetrically in the middle of the specimen. The strain evolution was recorded using a high-temperature extensometer.

The as-received material used in this study was a commercially produced AA7075 in temper T4 (solutionized and quenched, with natural aging) with a thickness of 2.0 mm. A PMI-MASTER direct-reading spectrometer was utilized to confirm the chemical composition of the sheet, as shown in Table 1. The geometry and dimensions of the tensile specimens are shown in Fig. 2. Specimens with a gauge length of 50.0 mm and a width of 5.0 mm were designed to achieve high

accuracy in the strain calculation and to adapt to the size of the heating furnace. To analyze the effect of anisotropy on the formability, tensile test specimens were cut by an EDM in three different directions along the RD (rolling direction), DD (diagonal direction) and TD (transverse direction) from the rolling direction of the sheet, as shown in Fig. 3.

Based on previous research results (Ref 9), the specimens were heated to 510 °C (optimum T_{SHT}) and solutionized for 30 min (optimum t_{SHT}) to ensure that the precipitated phase from the original state (T4) was fully redissolved into the matrix. The temperature tracking results obtained by the infrared thermometer showed that when the blank was transferred from the furnace to the blank holder, a Δt of 70 °C was obtained; i.e., the temperature at the center of the sheet dropped to 440 °C. For a realistic simulation of the convection during the blank transference and positioning, the specimens were cooled in ambient air for 15 s so that the temperature drop-down was implemented. The specimens then were cooled to the target temperature (T_i) using a high-pressure air rifle at a sufficient cooling rate. Two thermocouples were used at the two ends of the sample so that the temperature distribution at the different positions of the sample could be monitored at the same time to ensure the uniformity of the sample temperature.

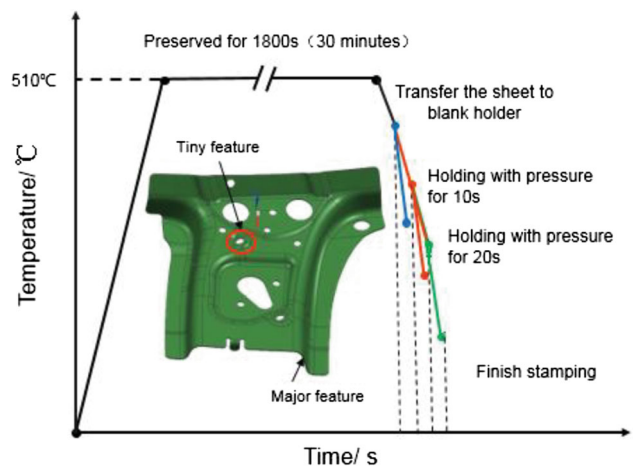


Fig. 8 Experimental program for the high-temperature hemispherical punch test based on the HFQ process under different initial forming temperatures

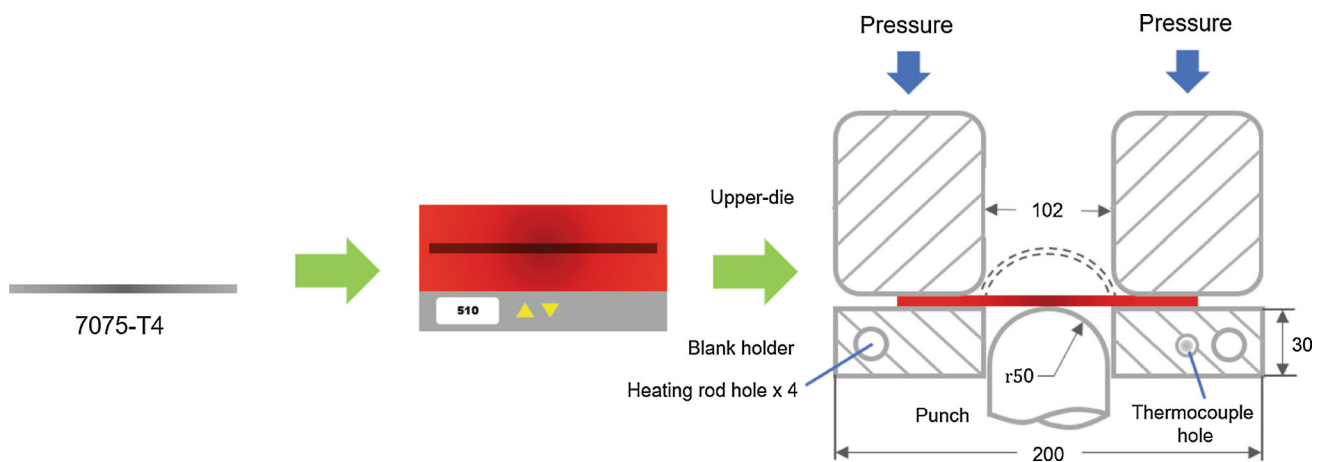


Fig. 7 Schematic of tools used in the high-temperature hemispherical punch test (unit: mm)

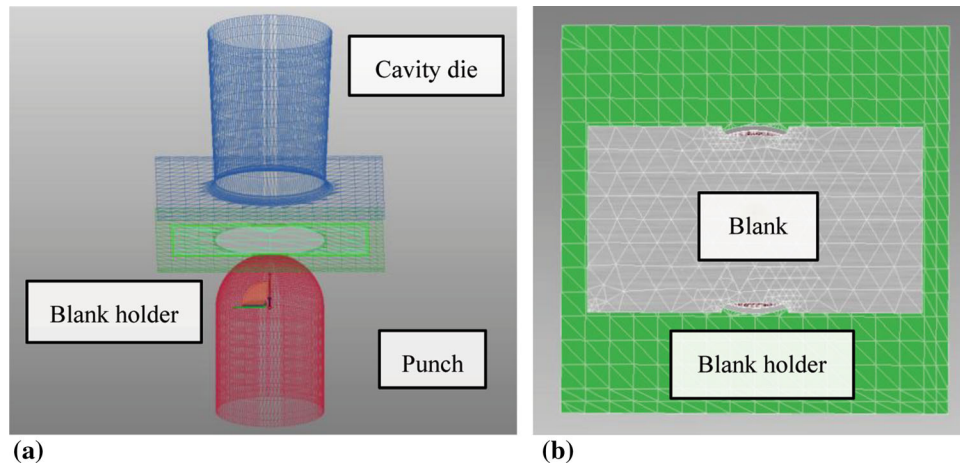


Fig. 9 FEM model in a mesh: (a) position relationship of the mold; (b) blank position

Table 2 Thermomechanical parameters of the 7075 aluminum alloy (Ref 20)

Temperature	Specific heat/(mJ/ton/K)	Thermal expansion/($1 \times 10^{-6} \text{ }^\circ\text{C}$)	Thermal conductivity/(mW/mm/K)
25	6.37E8	17.04	89
100	7.14E8	18.66	98
200	7.96E8	20.82	111
300	8.6E8	22.98	122
400	9.10E8	25.14	132
440	9.27E8	26.00	135

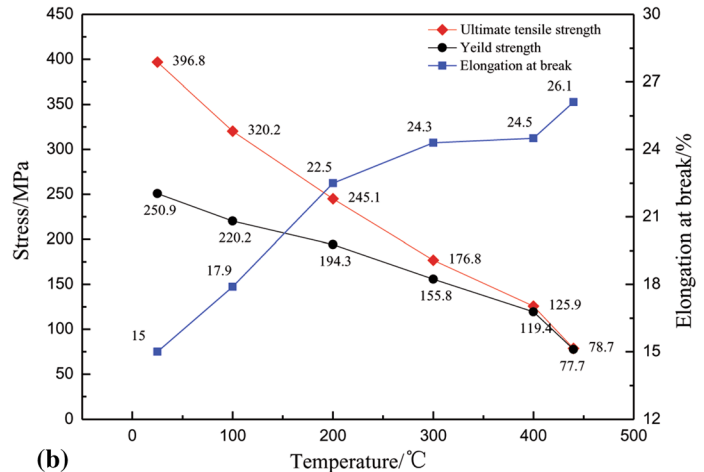
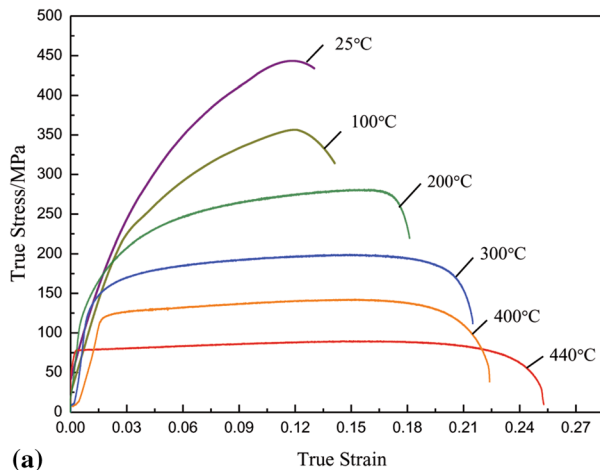


Fig. 10 Uniaxial tensile test results of 7075-T4 at various initial temperatures (strain rate: 0.01/s; specimen orientation: 0°). (a) True stress–true strain curve. (b) Mechanical properties

Finally, tensile tests were started and carried out until fracture. The experimental program is shown in Fig. 4.

Fracture surface samples were cut from the tensile specimens and then placed in acetone to remove oil and dirt using an ultrasonic cleaner for 10 min. Then, scanning electron microscopy (SEM) was used to observe the fracture morphology.

2.2 High-Temperature FLD Test

As the crucial indicator for assessing the sheet formability of 7075, a forming limit diagram (FLD) was studied using the

hemispherical punch test, which is a stamping test that allows a blank to be deformed until fracture or localized necking. The experimental standard was the Chinese standard GB/T15825.8-2016. Rectangular specimens with a uniform length of 180 mm but with different widths ranging from 20 to 180 mm at an increment of 40 mm were used to achieve different strain paths (biaxial tensile, plane strain tensile and uniaxial tensile), as shown in Fig. 5. To measure the major and minor strains after testing, the surface of each blank was electrochemically etched with circular grid patterns of 5 mm diameter.

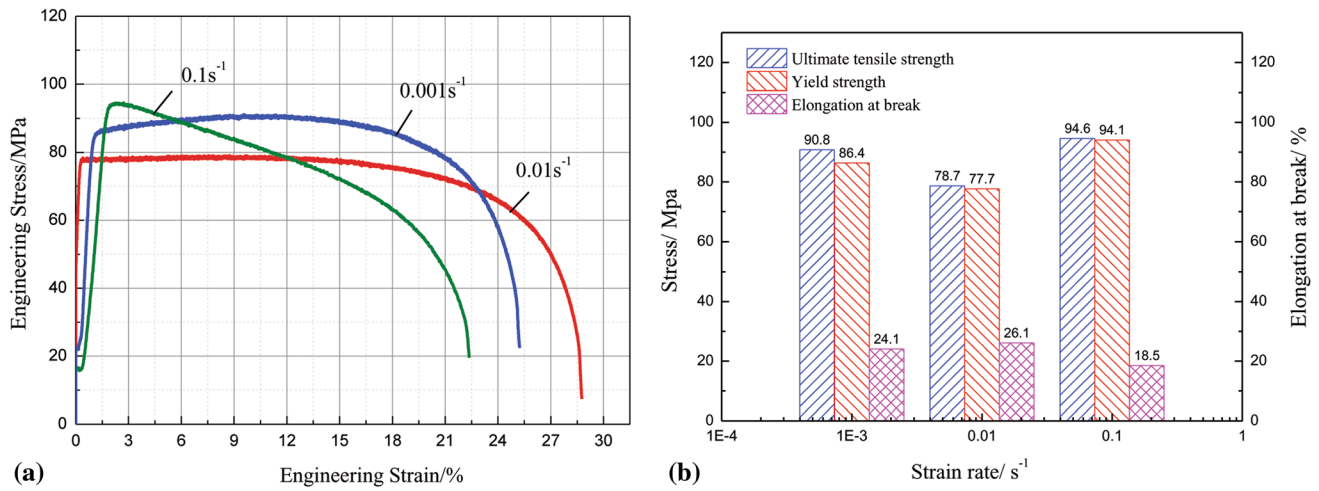


Fig. 11 Uniaxial tensile test results of 7075-T4 at various strain rates (initial temperature: 440 °C; specimen orientation: 0°). (a) Engineering stress–strain curve. (b) Mechanical properties

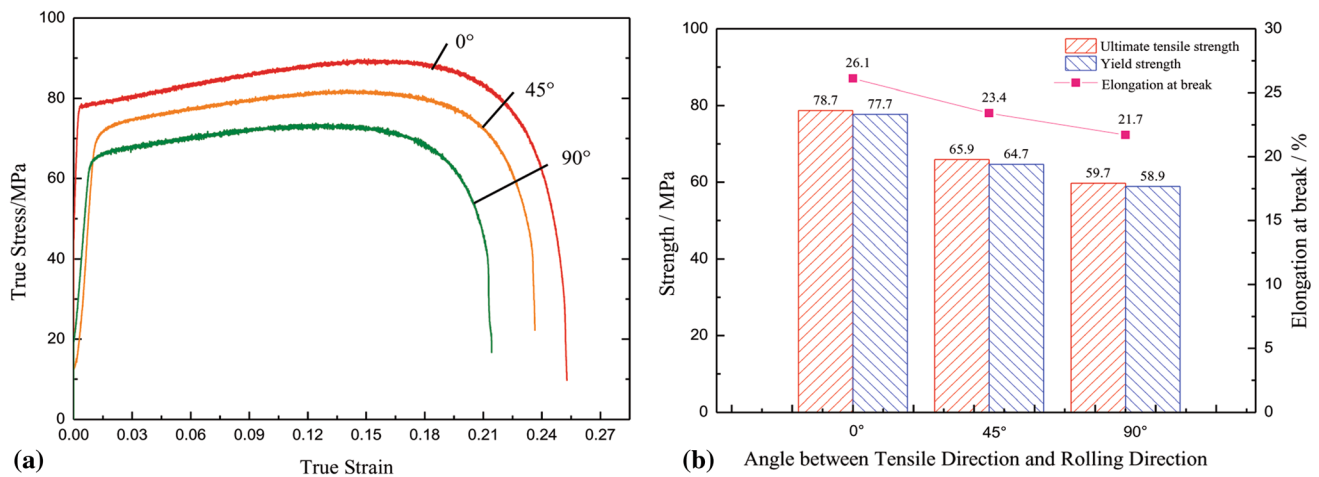


Fig. 12 Uniaxial tensile test results of 7075-T4 at various angles between the tensile direction and rolling direction (initial temperature: 440 °C; strain rate: 0.01/s). (a) True stress–true strain curve. (b) Mechanical property

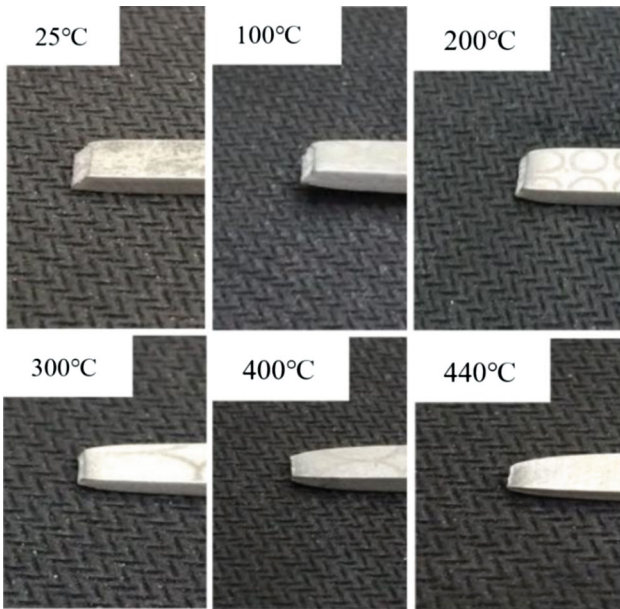


Fig. 13 Fracture morphology of the specimens

Table 3 ‘r’ value of 7075-T4 specimens at different rolling directions (440 °C, 0.01/s)

r_0	r_{45}	r_{90}	r	Δr
1.132	1.532	1.784	1.495	– 0.148

FLD tests were performed on a THP01-500A hydraulic press, and the test device was composed of a furnace, fixed hemispherical punch, upper die, blank holder with four embedded heating rods and an embedded thermocouple, as illustrated in Fig. 6. The schematic of the tools used in the high-temperature hemispherical punch test is shown in Fig. 7. A blanking holding force of 80 kN was applied to prevent the sheet from wrinkling. The blank holder was heated to a high temperature of 400 °C via the four heating rods to reduce the temperature loss during the blank transfer period. Each blank was heated to 510 °C for 30 min and rapidly transferred to the blank holder in only 15 s. The recommended forming rate was 0.01/s according to the high-temperature tensile test, as shown

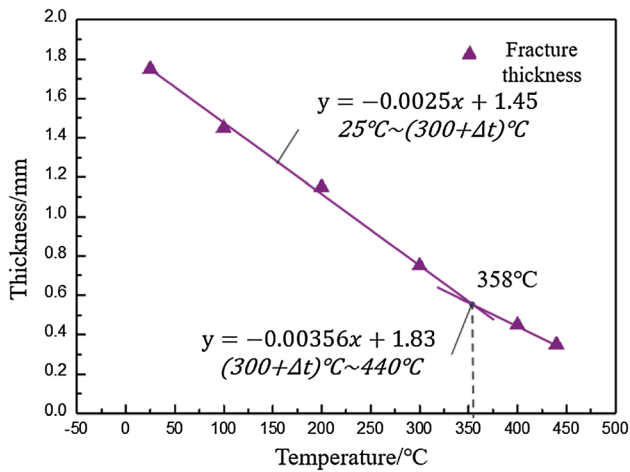


Fig. 14 Graphical calculation of the shear neck fracture transition temperature

in “High-Temperature Tensile Test” section. When the size of the specimen was 180×20 mm, the stress in the largest deformation zone was closest to the uniaxial tensile path. It was observed that when the strain rate was 0.01/s, the punch movement could be approximated as 10 mm/s.

In addition, it is necessary to take the initial forming temperature into consideration in nonisothermal stamping. For instance, some small characteristic structures, such as bosses or grooves of complicated components, start forming almost at the end of the stamping, giving rise to further temperature loss. This clear difference in the initial forming temperature between the different positions of the sheet has a distinct impact on the formability. Therefore, the initial forming temperature was controlled by adjusting the waiting time from 0 s to 20 s due to the constant forming speed, as illustrated in Fig. 8.

Square samples with a length of 10 mm that were mechanically cut from the sidewall of the hemispherical specimens were used to analyze the microstructure. The samples were etched in 10% NaOH for 10 min, followed by the use of 10% nitric acid to wash away the chemical reaction products on the surface. Eventually, the vertical-sectional microstructure of the samples was characterized by OM.

2.3 Numerical Simulation of the Temperature Field

The temperature field is vital for further investigations of the thermomechanical coupling effects during FLC tests. Since it is difficult to keep the thermal sensor intact due to the closed environment during stamping and the poor welding performance, measuring the temperature field of the 7075 aluminum alloy specimen during the forming process is not feasible. To better visualize the heat transfer between the 7075 aluminum alloy sheet and the tools, a temperature field simulation of the aluminum alloy stamping experiment process was carried out using the Autoform finite element simulation software. It was found that the Fields–Backofen exponential model that introduced the softening factor could better fit the true stress–true strain curves of the 7075 aluminum alloy sheet.

Figure 9 shows the FEM model of the forming tools and sheet blank in the simulations. The specimen was initially divided into 26 elements by an Automeshing due to its simple blank shape. The maximum element size was 40 mm, and the minimum element size was 0.33 mm near the fillet. The

Table 4 Thickness of the fracture location at different quenching temperatures in the tensile test (T_f : the thickness of the fracture)

Temperature/°C	RT	100	200	300	400	440
T_f /mm	1.75	1.45	1.15	0.75	0.45	0.35

thermodynamic properties are summarized in Table 2. The friction coefficient of 0.65 was measured by the high-temperature friction test, and the blank holder force was 80 kN. The tool material was specified as H13 steel, and the IHTC value between them was set as $3300 \text{ W/m}^2 \text{ K}$ (Ref 8). The hardening curves at RT and elevated temperatures were extracted from the constitutive model of the 7075 aluminum alloy that reflected the law of the material’s rheology during the plastic deformation stage. Specimens under the plane strain path with a sheet size of $180 \text{ mm} \times 100 \text{ mm}$ were selected for the temperature field simulations.

3. High-Temperature Mechanical Properties

3.1 Influence of Temperature

A series of true stress–strain curves at different temperatures is shown in Fig. 10. We use the tensile testing result at 440 °C as an example. The curve can be divided into four stages: (I) the hardening stage, (II) the homogeneous deformation stage, (III) the diffusion necking stage and (IV) the localized necking stage. It is apparent that stage (I) narrowed as the temperature increased. Moreover, stage (II) of the curves gradually tended to steady the flow characteristic when the temperature increased above 300 °C, demonstrating a dynamic balance between the hardening effect due to sharp dislocation accumulation and the softening effect due to dynamic recovery or dynamic recrystallization. For a further comparison, the mechanical properties, e.g., yield strength, ultimate tensile strength and elongation to fracture, were extracted from the true stress–strain curves. The yield strength and the tensile strength gradually decreased with increasing temperature while the elongation at break steadily rose from RT to 440 °C. It is well known that elongation to fracture is a significant indicator of a material’s plasticity. The maximum value reached 26.1% at 440 °C, which is 74% higher than the elongation to fracture at RT, indicating a clear formability improvement when adopting the HFQ process.

3.2 Influence of the Strain Rate

Figure 11 shows the engineering stress/strain curves and mechanical properties under different strain rates, and it is observed that the difference between these flow curves also strongly depends on the strain rate. When the strain rate increased from 0.01 to 0.1/s, the tensile strength increased by approximately 16 to 94.6 MPa and the elongation at break decreased by 7.6%, showing a positive correlation with the strain rate. When the strain rate was 0.1/s, the stress–true strain curve reached peak stress at the initial stage of stretching and was significantly higher than the peak stress at the other strain rates due to the higher strain rate. The dislocations were not as good as the movement, and the plugging was increased,

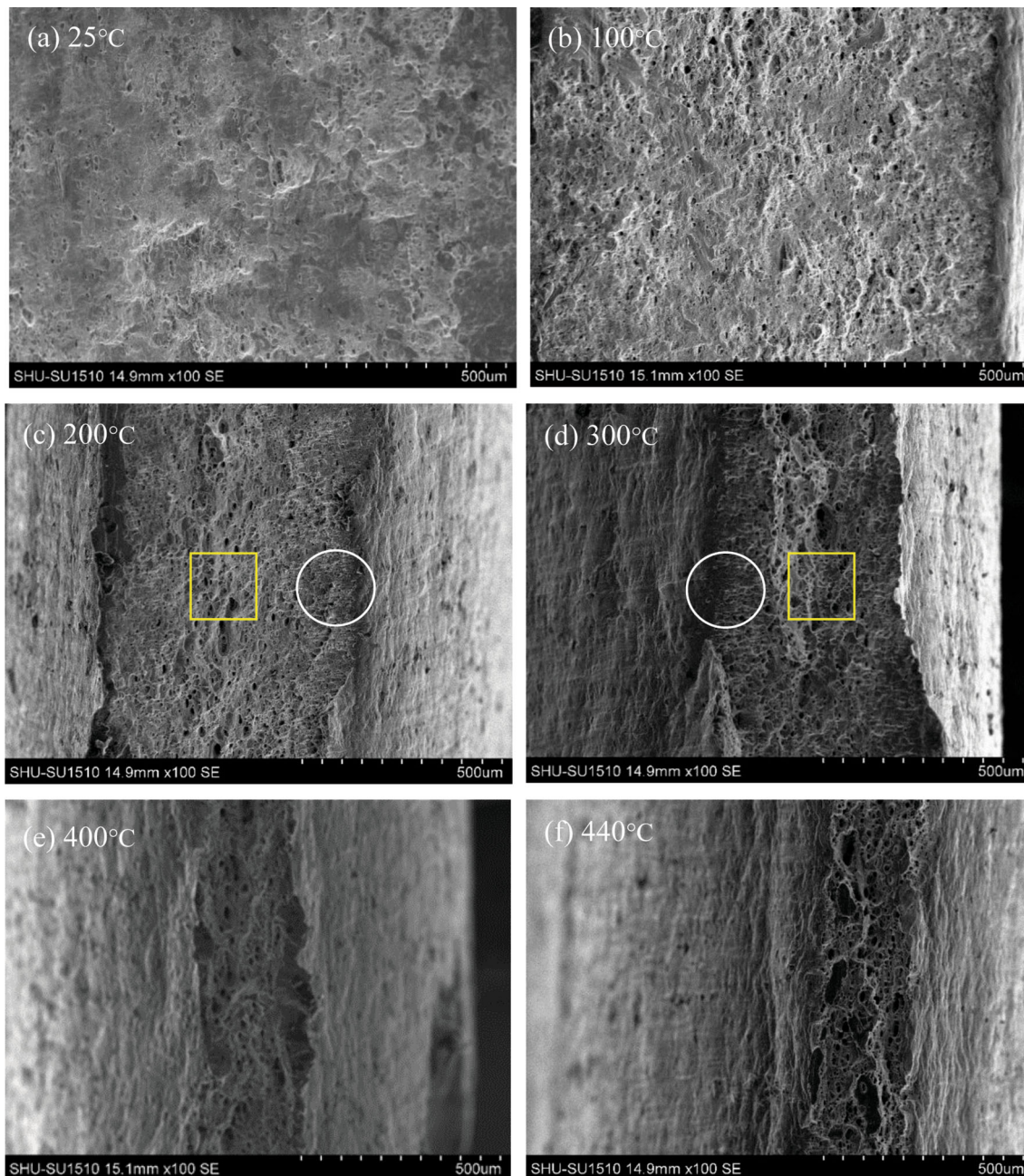


Fig. 15 Fracture morphology of the specimens at $\times 100$ magnification. (a) 25 °C. (b) 100 °C. (c) 200 °C. (d) 300 °C. (e) 400 °C. (f) 440 °C

increasing the deformation resistance of the sheet. Generally, since the piling up of the dislocations accelerated due to the increasing strain rate, the deformation storage energy of the 7075 alloy increased, presenting an increasing strength from the macroscopic point of view. In contrast, a lower strain rate provided a sufficient time for the softening behavior, e.g., dynamic recrystallization, to exhaust the stored energy. In addition, stage (II) of the flow stress curve at 0.1/s showed a downward trend, indicating that the softening effect caused by the temperature far exceeded the hardening effect, which can probably be attributed to the occurrence of dynamic recrystallization over a higher deformation temperature range. Nevertheless, when the strain rate increased from 0.001 to 0.01/s, the tensile strength decreased by approximately 12 MPa and the elongation at break increased by 2%, indicating a negative

correlation with the strain rate. The tensile temperature at 0.001/s was lower than that at 0.01/s under each strain, explaining why the plasticity of the 7075 aluminum alloy sheet increased with the increase in the strain rate in hot stamping.

3.3 Influence of Plastic Anisotropy

Since the as-received sheet primarily experienced a rolling process, texture structures were formed in the alloy sheets, exhibiting macroscopic anisotropy. The flow stress curves and mechanical properties in all three directions are shown in Fig. 12. It is observed that the RD has the highest values of the mechanical properties, including yield strength (77.7 MPa), ultimate tensile stress (78.7 MPa) and elongation to fracture (26.1%), compared to those in the DD and TD directions. *R*-bar

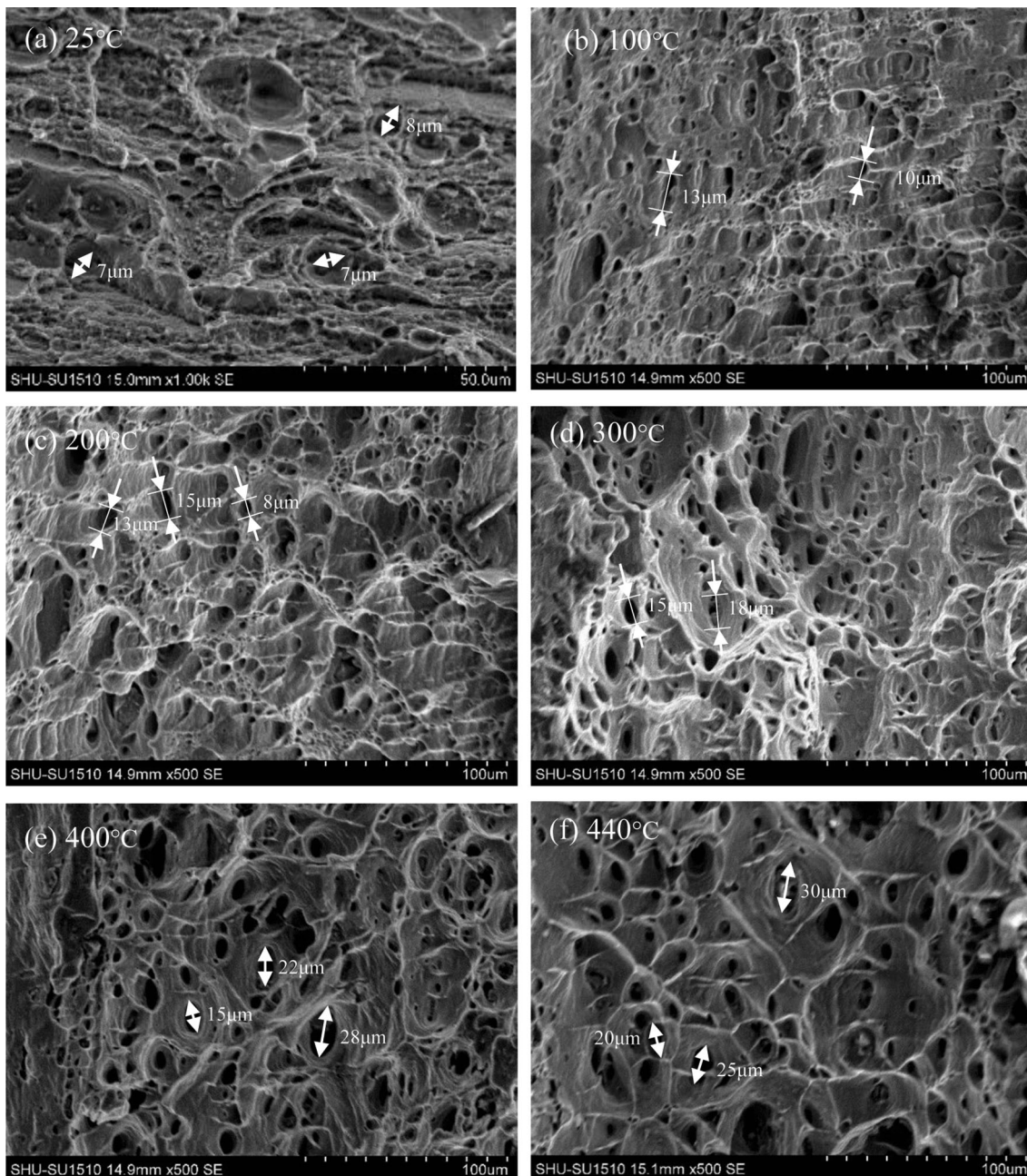


Fig. 16 Fracture morphology of the specimens at $\times 500$ magnification. (a) 25 °C. (b) 100 °C. (c) 200 °C. (d) 300 °C. (e) 400 °C. (f) 440 °C

tests were subsequently conducted to determine the plastic anisotropy index (r' value) of the alloy sheet in different directions. Although a few studies on plastic anisotropy of 7075 at RT have been performed by Senthil et al. (Ref 21), it is still necessary to explore the anisotropy index at elevated temperature. Generally, a sheet metal with a higher r' value has higher formability. Zhou et al. (Ref 22) found that the r' value increased with increasing temperature and that the r' value of 7075 was greater than 1 when the temperature exceeded 250 °C. It should be noted that when the r' value exceeds 1, the deformation takes place more easily along the plane direction than along the thickness direction. In this study, the highest r' value (1.784) was observed in the TD direction, whereas the

lowest r' value (1.132) was in the RD direction at 440 °C, which was in accordance with the trend observed in the previous study.

3.4 Fracture Mechanism

There was no obvious plastic deformation near the fracture surface when the quenching temperature decreased below 300 °C, as shown in Fig. 13. The rupture mode showed a typical shear fracture (45° diagonal-to-tensile direction) from RT to 300 °C, while the edge of the fracture surface of the specimen presented a zigzag characteristic due to tearing from 400 to 440 °C, which was a typical necking ductile fracture.

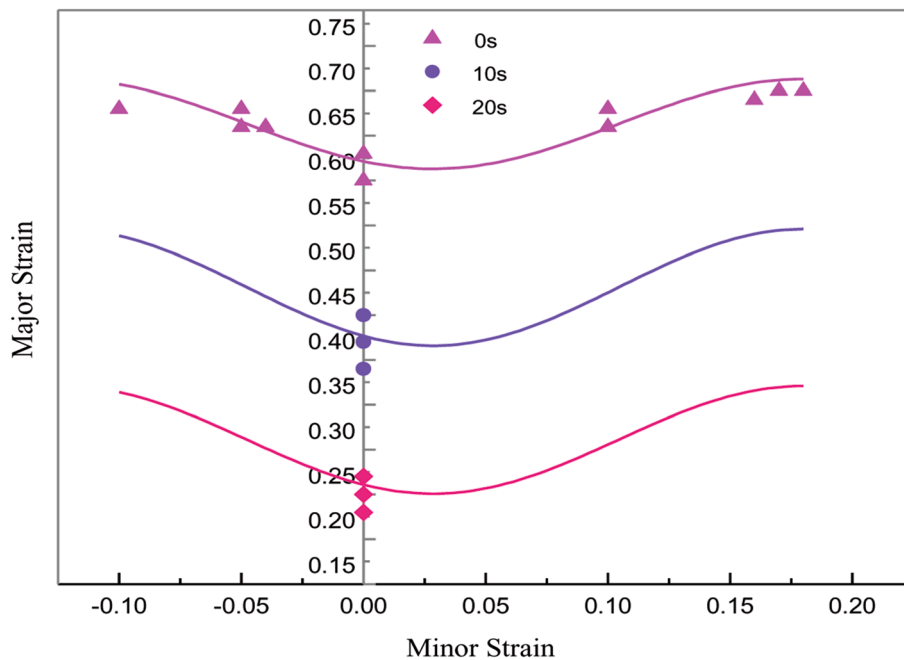


Fig. 17 Forming limit curves of 7075-T4 based on the HFQ process under different waiting temperatures with a forming velocity of 10 m/s

The thickness of the sectional area was measured to study the fracture mode evolution with different quenching temperatures, as shown in Table 3. The fracture thickness gradually increased with the decrease in the initial tensile temperature. By further comparing the relationship between the temperature and fracture thickness, it was found that the relationship between the thickness and temperature is linear under different fracture behaviors. The relationship between the cross-sectional thickness and temperature is approximately $y = -0.0025x + 1.45$ [$25\text{ }^{\circ}\text{C} \sim (300 + \Delta t)$] $^{\circ}\text{C}$ and $y = -0.00356x + 1.83$ [$(300 + \Delta t) \sim 440$] $^{\circ}\text{C}$, as obtained by linear fitting, which is illustrated in Fig. 14. The ductile shear-necking fracture transition of 7075 based on HFQ occurred at $358\text{ }^{\circ}\text{C}$, as obtained by calculating the intersection point of two straight lines (Table 4).

The fracture morphologies of the specimens at different temperatures are shown in Fig. 15 and 16 to justify the fracture mechanism. Microscopic voids were generated and distributed on the flat fracture surface, as shown in Fig. 15(a), at a relatively low deformation temperature. It is observed that the equiaxial dimples invariably focused on the center of the specimen surface (square area), while the parabolic dimples were distributed at the edge of the fracture (circle area), indicating that the edge of the fracture was under tear stress. Furthermore, the microstructure magnification was amplified to higher multiples for further observations, as illustrated in Fig. 16. The number of dimples on the surface rapidly increased and the average diameter of equiaxial dimples clearly grew to $25\text{ }\mu\text{m}$ at $440\text{ }^{\circ}\text{C}$, implying that the coalescence of the dimples was most likely to occur with increasing temperature. Broken second-phase particles were observed in the bottom of the dimples (Ref 9). The generation of these irregular particles can lead to the initiation of microcracks due to the greater stress concentration. It is thus concluded that the nucleation, growth and aggregation of cavities are responsible for the fracture in the tensile tests (Fig. 17).

4. High-Temperature Forming Limit Properties

4.1 FLC_0 Under Different Initial Forming Waiting Times

Since the simulation is under the plane strain path, the major strain approached the middle region (the lowest point) of the FLC curve when the fracture was initiated. The intersection of FLC and y-axis, namely FLC_0 , generally considered to be the lowest point of FLC, is introduced in this section. To reduce the large number of unnecessary experiments, only FLC_0 values are used to study the trends of the forming limit at different waiting times.

The variation of the vertical position among three FLC points illustrated that the initial forming temperature had a pronounced influence on the formability of the 7075 aluminum alloy. When the waiting time was extended to 10 s, the major strain of FLC_0 value markedly decreased to 0.42; as the waiting time increased to 20 s, the height position of the FLC_0 value decreased to 0.25. In summary, with increasing waiting time, FLC_0 decreases significantly in the vertical position.

4.2 Numerical Simulation of the Temperature Field

FEM simulations were carried out to further investigate the thermomechanical coupling effect of the 7075-T4 aluminum alloy sheet in the high-temperature FLD test. Temperature evolution histories depending on the stamping stroke were extracted from the simulations at different waiting times, as displayed in Fig. 18. When the sheet was just transferred to the blank holder from the furnace, the alloy sheet temperature dropped from the initial temperature of $510\text{ }^{\circ}\text{C}$ to a maximum temperature of $445\text{ }^{\circ}\text{C}$ in the center and a minimum temperature of $437\text{ }^{\circ}\text{C}$ at the edge, in good agreement with the experimental results. The temperature distribution of the 7075-T4 aluminum alloy sheet during hot stamping was influenced by different waiting times on the blank holder. When the 7075

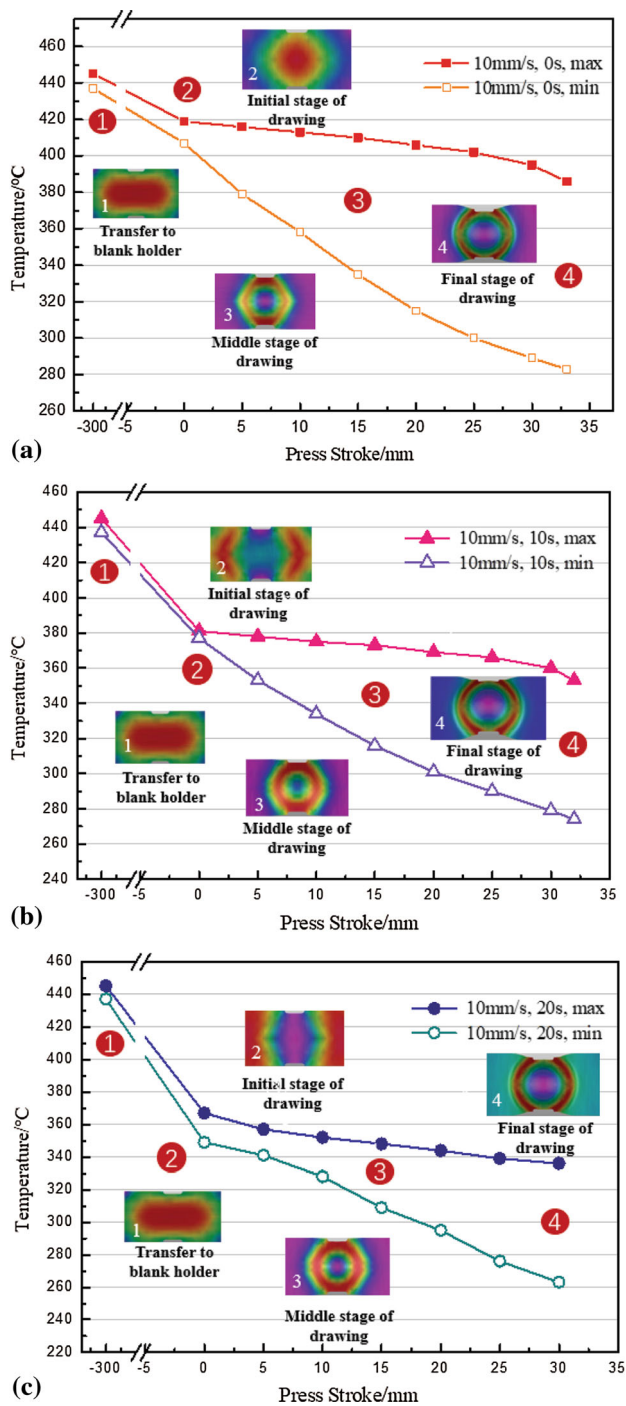


Fig. 18 Absolute temperature–press stroke curves of the 7075 deformed sheet at different waiting times: (a) 0 s. (b) 10 s. (c) 20 s

aluminum sheet was transferred to the blank holder from the furnace, the overall temperature of the sheet was higher than the heated blank holder temperature of 400 °C. During the period of waiting for the cavity die to descend, heat conduction between the blank holder and the sheet resulted in a temperature loss in the marginal zone. The lowest temperature of the marginal zone of the sheet was 407 °C, and the central temperature was naturally cooled to 419 °C in air. When the sheet was placed on the blank holder and left for some amount of time prior to ram motion, the heat conduction between the sheet and the blank holder was lower due to the decreasing

temperature difference between them. The temperature reduction in the marginal region increased more slowly, while the temperature of the central region steadily dropped due to continuous air convection. When the waiting time was set to 10 s, it was observed that the difference between the maximum temperature and the minimum temperature was only 4 °C in the initial stage of stamping. As the waiting time was further extended to 20 s, the temperature at the edge of the sheet dropped to 367 °C. The temperature in the central zone decreased to 349 °C due to thermal convection with air, and the temperature distribution appeared to be opposite that shown in Fig. 18(a) and (b). When the aluminum alloy sheet moved into the bulging stage, the temperature in the central zone rapidly decreased because of the contact with the cold punch. The lowest temperature zone always occurred at the top zone of the hemispherical part, and the highest temperature appeared in the final bulging zone of the sheet. As the waiting time increased, the difference between the maximum and minimum temperatures in the final stage of drawing narrowed, and the temperature range became increasingly narrow (Fig. 19).

4.3 Crack Specimens

To further investigate the effect of thermomechanical coupling on the rupture behavior of the 7075-T4 part in hot stamping, the fracture morphology and microstructure under the fracture of 180 × 100 mm specimens stamped at different waiting times were observed, as shown in Fig. 20. In the high-temperature FLD test, the aluminum sheet contacts the punch from the center to the edge under the punch force. When the waiting time was 0 s, the lowest initial forming temperature of 407 °C occurred in the marginal region of the sheet and the initial forming temperature of the final bulging zone was 381 °C, as shown in Fig. 19. The main deformation zone gradually transferred from the top region to the sidewall in a bulging deformation. The main deformation zone obtained a sufficient metal supplement from the surrounding metal due to the increasing temperature gradient from top to bottom. The local instability finally occurred at a lower position, resulting in a necking fracture. When the waiting time was 10 s, the rupture position slightly decreased, also showing a necking fracture. The rupture position moved upward when the waiting time was extended to 20 s. The initial forming temperature of the bulging zone decreased to the range of 348 to 352 °C, and the temperature gap at each forming stage decreased. As described in “Fracture Mechanism” section, when the initial forming temperature dropped below 358 °C, the deformation resistance of the 7075-T4 aluminum alloy sheet significantly increased. A ductile shear fracture occurred at a higher position in the sidewall and spread only in the horizontal direction, which is consistent with the NTSF transition regulation in the high-temperature tensile test. The rupture did not occur in the effective zone due to the concentrated deformation in the cavity die circular-arc resulting from the increasing temperature gap between the flange and the central zone in the initial stage, as inferred from the trend of the temperature field shown in Fig. 18.

Since the fracture morphology also plays an important role in the analysis of the failure mode, the cracks of the specimens at different die temperatures were observed using scanning electron microscopy (SEM). Figure 21(b) shows that when the waiting time is extended to 10 s, the fracture morphology still maintains the similar characteristics of tearing dimples to those

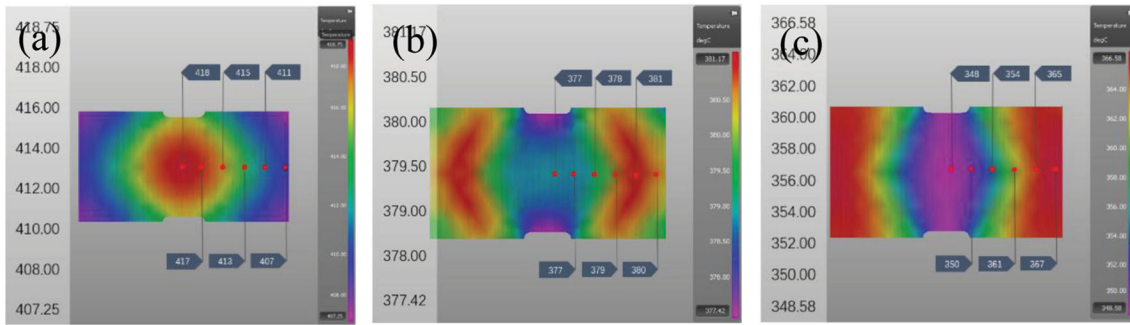


Fig. 19 Absolute initial forming temperature distribution of the 7075 aluminum alloy sheet at different waiting times: (a) 0 s. (b) 10 s. (c) 20 s

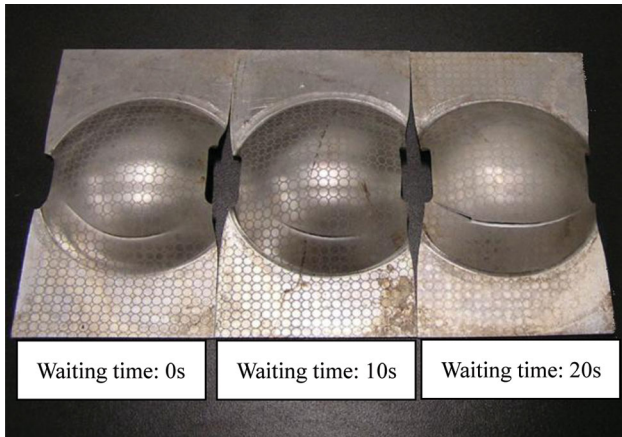


Fig. 20 Deformed specimens at different waiting times

obtained under the 0 s waiting time. The dimples show a clear directionality due to the tearing force exerted from the upper die and punch to the 7075-T4 alloy sheet. However, the quantity and size of the average dimples significantly decreased, and the average dimple size decreased from 26 to 20 μm , indicating that the plasticity of the 7075-T4 alloy sheet was slightly lower than that of the sheet when the waiting time was extended from 0 to 10 s. Figure 21(c) shows that when the waiting time was extended to 20 s, the dimples on the fracture surface were very small, and the average size was only 11-12 μm . The morphology of the dimples changed from the previous tearing mode into the orthogonal mode, indicating that the deformation resistance of the sheet evidently increased under a waiting time of 20 s.

Different fracture modes under different initial stamping temperatures correspond to different local microstructure, as shown in Fig. 22. The microstructure at a waiting time of

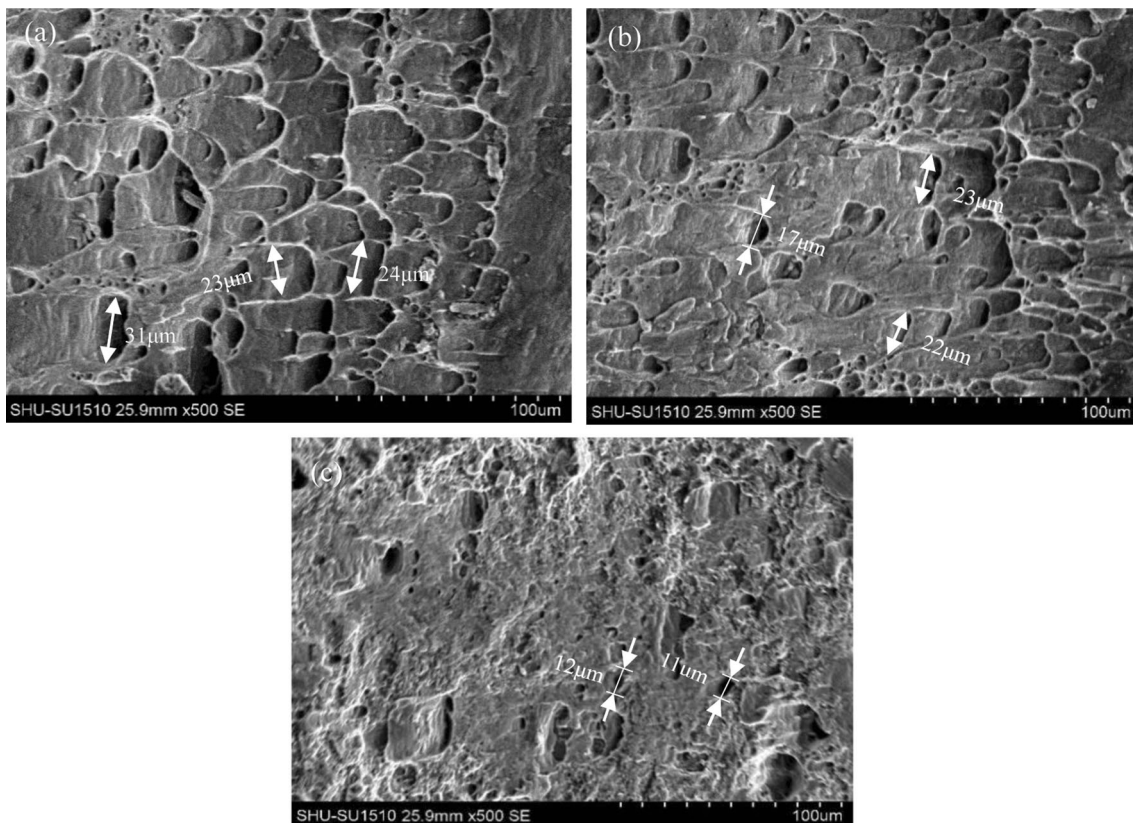


Fig. 21 Fracture morphology under different initial forming times: (a) 0 s. (b) 10 s. (c) 20 s

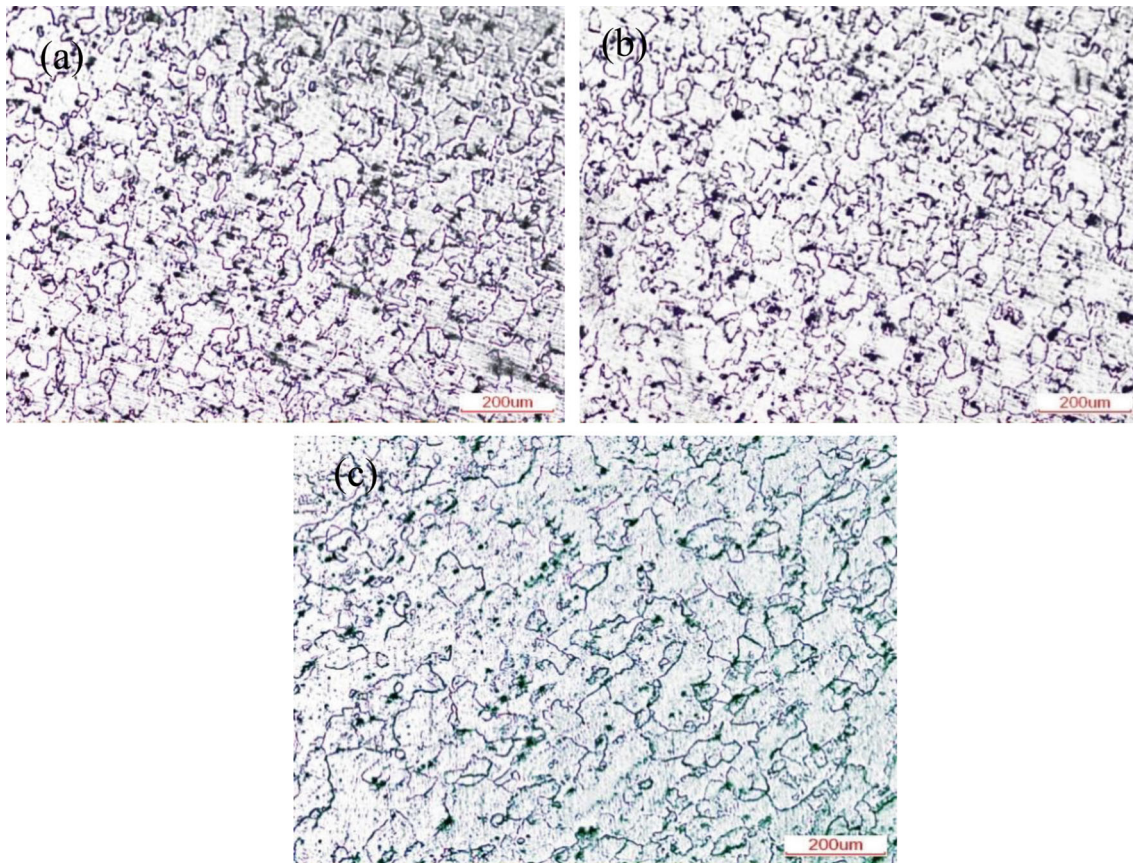


Fig. 22 Vertical-sectional microstructure of the FLC specimens adjacent to the crack region under different waiting times: (a) 0 s. (b) 10 s. (c) 20 s

20 s mainly consists of coarse grains mixed with small equiaxial grains, as shown in Fig. 22(a). Comparing Fig. 22(b) and (c), it is observed that the proportion of fine equiaxial grains dramatically increases with increasing waiting time, demonstrating that increasing the initial forming temperature causes the development of the DRX to be more thorough. The specific fraction of recrystallized grains was computed to be 0.37, 0.30, and 0.19. The transition from a necking fracture to a ductile shear fracture among the three test conditions can also be explained by the higher degree of DRX of the sidewall at waiting times of 0 and 10 s. In addition, it is remarkable that the vertical position of FLC at 10 mm/s with no waiting time is approximately 2.8 times higher than that at a waiting time of 20 s, which can be explained by the appearance of dynamic recrystallization (DRX) at high temperature. Sakai et al. (Ref 23) found that the structural changes of the 7000 series aluminum alloy consisted of the development of microshear bands during early deformation followed by a homogeneous evolution of new grains, showing a continuous dynamic recrystallization (CRDX) mechanism.

5. Conclusions

In the present study, the mechanical properties, fracture morphology and microstructure of a 7075-T4 aluminum alloy sheet obtained from the high-temperature tensile test and FLD

test were investigated in detail. The conclusions that were drawn are as follows:

1. The tensile strength decreases from 396.8 MPa in the quenched state to 78.7 MPa when the stretching temperature is increased from room temperature to 440 °C, and the elongation at break slowly increases with increasing temperature, from 15% in the quenched state to 26.1% at 440 °C, for an increase of 74%.
2. The ductile shear-necking fracture transition of 7075 based on HFQ occurred at 358 °C. Under high-temperature tensile tests, the fracture mechanism is that of micro-pore aggregation fracture.
3. The forming limit of 7075-T4 evidently dropped with increasing waiting time. The optimized FLC₀ value of 7075-T4 at a waiting time of 0 s is 0.6, showing higher drawability and bulgeability.
4. When the waiting time was set to 0 s, the rupture type of the actual stamping specimen was the necking mode. When the blank waiting time was increased to 20 s, the fracture belonged to the shear mode, which is consistent with the NTSF transition temperature in the high-temperature tensile test.
5. The local microstructure becomes nonuniform due to the temperature distribution, finally resulting in different fracture modes. The change from a ductile necking fracture to a shear fracture in the sidewall can also be explained by the higher DRX degree of the specimens at waiting times of 0 and 10 s.

Acknowledgments

The joint support from the National Natural Science Foundation of China (Grant No. 51475280) and the Shanghai Automotive Industry Science and Technology Development Fund (Grant No. 1610) is gratefully acknowledged.

References

1. T. Dursun and C. Soutis, Recent Developments in Advanced Aircraft Aluminium Alloys, *Mater. Des.*, 2014, **56**, p 862–871
2. R.P. Garrett, J. Lin, and T.A. Dean, Solution Heat Treatment and Cold Die Quenching in Forming AA 6xxx Sheet Components: Feasibility Study, *Adv. Mater. Res.*, 2005, **6–8**, p 673–680
3. O. Fakir, L. Wang, and D. Balint, Numerical Study of the Solution Heat Treatment, Forming, and In-die Quenching (HFQ) Process on AA5754, *Int. J. Mach. Tools Manuf.*, 2014, **87**, p 39–48
4. B. Mostefa, A. Abdelkrim, B. Ali, and B. Mohamed, Effect of Hardening Induced by Cold Expansion on Damage Fatigue Accumulation and Life Assessment of Aluminum Alloy 6082 T6, *Mater. Res.*, 2012, **15**, p 981–985
5. L. Ying, T. Gao, M. Dai, and P. Hu, Investigation of Interfacial Heat Transfer Mechanism for 7075-T6 Aluminum Alloy in HFQ Hot Forming Process, *Appl. Therm. Eng.*, 2017, **118**, p 266–282
6. L. Ying, W.Q. Liu, and D.T. Wang, Experimental and Simulation of Damage Evolution Behavior for 7075-T6 Aluminum Alloy in Warm Forming (in Chinese), *Chin. J. Nonferrous Metals*, 2016, **26**, p 1383–1390
7. Y.L. Zheng, C.G. Yan, and P.Q. Si, Microstructure and Performance of Top-forged Friction Plug Welding Joint of 7075-T6 Aluminum Alloy (in Chinese), *Hot Work. Technol.*, 2018, **47**, p 90–93
8. L. Ying, T. Gao, and M. Dai, Investigation of Interfacial Heat Transfer Mechanism for 7075-T6 Aluminum Alloy in HFQ Hot Forming Process, *Appl. Therm. Eng.*, 2017, **118**, p 266–282
9. Q. Liu, S. Chen, R. Gu, W.R. Wang, and X.C. Wei, Effect of Heat Treatment Conditions on Mechanical Properties and Precipitates in Sheet Metal Hot Stamping of 7075 Aluminum Alloy, *J. Mater. Eng. Perform.*, 2018, **27**, p 4423–4436
10. Y.C. Yan, Flow Stress Constitutive Equation of 7050 Aluminum Alloy during Hot Compression Deformation (in Chinese), *J. Mater. Eng.*, 2007, **4**, p 20–22
11. S. Gourdet and F. Montheillet, An Experimental Study of the Recrystallization Mechanism During Hot Deformation of Aluminium, *Mater. Sci. Eng. A*, 2000, **283**, p 274–288
12. W.M. Zhuang, Prediction of Hot Stamping Limit of 7075 Aluminum Alloy Based on Continuous Medium Damage Mechanics (in Chinese), *J. Jilin Univ. (Eng. Sci.)*, 2014, **44**(02), p 409–414
13. K. Senthil, M.A. Iqbal, P.S. Chandel, and N.K. Gupta, Study of the Constitutive Behavior of 7075-T651 Aluminum Alloy, *Int. J. Impact Eng.*, 2017, **108**, p 171–190
14. W. Huo, L. Hou, Y. Zhang, and J. Zhang, Warm Formability and Post-forming Microstructure/Property of High-Strength AA 7075-T6 Al Alloy, *Mater. Sci. Eng. A*, 2016, **675**, p 44–54
15. V.K. Barnwal, R. Raghavan, A. Tewari, K. Narasimhan, and S.K. Mishra, Effect of Microstructure and Texture on Forming Behavior of AA-6061 Aluminum Alloy Sheet, *Mater. Sci. Eng. A*, 2016, **679**, p 56–65
16. S.P. Keeler, Determination of Forming Limits in Automotive Stampings. SAE Technical Paper, 1965
17. G.M. Goodwin, Application of Strain Analysis on Sheet Metal Forming Problems in the Press Shop. SAE Technical Paper, 1968
18. H. Hua, *Experimental and Theoretical Investigation of Warm Forming of High-strength Aluminum Alloy Sheet (in Chinese)*, Shanghai Jiaotong University, Shanghai, 2010
19. M. Mohamed and D. Szegda, An Industrial Application of the Continuum Damage Mechanics (CDM) Model for Predicting Failure of AA6082 Under HFQ Process, *Procedia Eng.*, 2017, **183**, p 277–282
20. X. Liu, K. Ji, O.E. Fakir, H.M. Fang, M.M. Gharbi, and L.L. Wang, Determination of the Interfacial Heat Transfer Coefficient for a Hot Aluminium Stamping Process, *J. Mater. Process. Technol.*, 2017, **247**, p 158–170
21. K. Senthil, M.A. Iqbal, P.S. Chandel, and N.K. Gupta, Study of the Constitutive Behavior of 7075-T651 Aluminum Alloy, *Int. J. Impact Eng.*, 2017, **108**, p 171–190
22. J. Zhou, J. Zhang, and P. Ji, Crystal Orientation Evolution of Friction Stir Welding of 2024/7075 Dissimilar Aluminum Alloys, *Trans. China Weld. Inst.*, 2016, **37**, p 59–62
23. T. Sakai and C. Takahashi, Flow Softening of 7075 Aluminum Alloy Under Hot Compression, *Mater. Trans. JIM*, 1991, **32**, p 375–382

Publisher's Note Springer Nature remains neutral with regard to jurisdictional claims in published maps and institutional affiliations.